METROLOGY AND MEASUREMENT SYSTEMS
Index 330930, ISSN 0860-8229
www.metrology.pg.gda.pl

THE APPLICATION OF INVERSE ANALYSIS IN STRAIN DISTRIBUTION RECOVERY USING THE FIBRE BRAGG GRATING SENSORS

Waldemar Wójcik, Piotr Kisała

Lublin University of Technology, Department of Electronics, Nadbystrzycka 38A, 20-618 Lublin, Poland (✉ p.kisala@pollub.pl, +48 81 5384 311, *waldemar.wojcik@pollub.pl)*

Abstract

This paper outlines the use of inverse analysis in strain distribution recovery. To carry it out we used a sensor with FBG (fibre Bragg grating) and the inverse problem solution was discussed. The study and validation of a mathematical model with the fibre Bragg grating is also outlined in this paper. Computer simulations were carried out using numerical algorithms which performed calculations according to the mathematical structure of the model and respected all remaining values of the FBG sensor elements. Experimental measurements were also conducted using a built measurement system.

Keywords: forward problem, inverse analysis, fibre Bragg gratings, strain distribution.

1. Introduction

Sensors based on fibre Bragg gratings have been used in metrology and measurement systems for years. They have a number of advantages such as: electromagnetic interference insensitivity, small mass and size, great sensitivity, a broad measurement band, and ease of transmission of light [1]. Thanks to their multiplexing capacity, measurements in many points and their application in WDM (Wavelength Division Multiplexing) and smart WDM systems are possible [2]. In many papers published recently, strain distribution in the grating using the finite element method, as well as the nonlinear deformations influence on the grating spectra were analyzed [3, 4]. Paper [5] provides an overview of the application of FBG sensors in strain measurement, particularly in the field of structural sensing.

In many papers, for instance [6], the embedding methodology in thin woven composites (thickness of 400 μm) was outlined. In the same paper, weave composite plates were used for sensor patch manufacturing. Two different configurations were considered and compared: carbon fibre/epoxy glue and glass fibre/epoxy glue plates. Unfortunately the results of this study could only be related to a specific specimen, while in this paper we propose many different specimen shapes to analyze the material behaviour and strain distribution recovery.

In most studies the grating is embedded by the epoxy glue [7]. FBG sensors have been also embedded in a variety of advanced composite materials [8]. This requires an examination of the FBG spectra before and after the fabrication process.

In our study the grating was surface-bonded to many different specimens using an adhesive. Moreover we used the sikadur-30 glue whose Young modulus is 13 GPa, while a typical bonding layer Young modulus is 3-3,5 GPa [9]. Such a high Young modulus of this glue increases the strain transmission rate to the FBG element.

In many studies the shape of strain distribution is similar (only the strain amplitude changes) [6]. We designed and constructed a special instrument and special specimens (each specimen of a different shape) to generate unique strain distribution shapes in fibre Bragg

gratings. The uniqueness and variety of shapes allowed us to characterize the accuracy of the strain distribution recovery depending on the distribution shape. There was a relationship between the shape and the recovery accuracy of strain distribution.

2. Method

In this article the use of an inverse problem [10] for the strain distribution recovery with the use of the fibre Bragg grating was outlined. The problem of strain profile recovery on the basis of the grating spectrum is the so-called inverse problem. There are no analytical methods for the recovery of the grating strain distribution on the basis of its spectrum. Due to this situation, the following procedure was used (Fig. 1). First, the initial values of the strain distribution were assumed. These values were then used as input data to build a grating model. This model allowed us to calculate the optical spectrum and then this spectrum was compared with the measured grating spectrum. Next, the convergence criterion between these two spectra was checked. If convergence occurred, the optimal strain distribution was obtained. If no convergence occurred, the objective function (which was calculated on the basis of equation (1) was minimized and strain values were selected according to the simulated annealing (SA) algorithm:

$$FC = \sqrt{\frac{1}{m}\sum_{i=1}^{m}\left(\frac{T_m - T_c}{T_c}\right)^2}, \tag{1}$$

where FC is the objective function, T_m denotes the measured transmission spectrum of the grating and T_c denotes the calculated transmission spectrum (using the simulated annealing algorithm).

2.1. Measurement methodology

Fig. 1 shows the procedure of the strain distribution recovery on the basis of the measured Bragg grating spectrum.

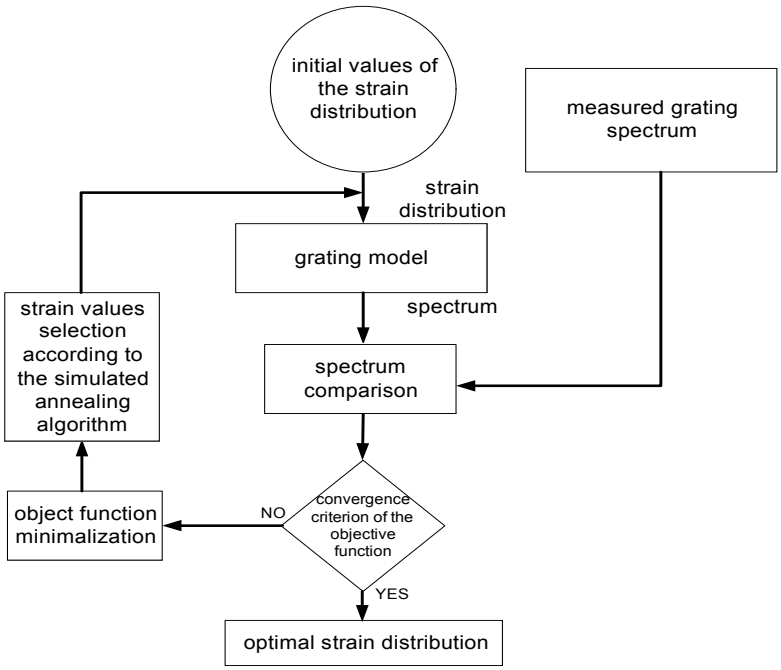

Fig. 1. The strain distribution recovery procedure.

The following were the three most important elements of the procedure depicted in Fig. 1: fibre Bragg grating model, the objective function and its minimization algorithms. A general classification of inverse methods with examples of techniques belonging to particular groups was presented in article [11], whose authors studied inverse problems in indirect measurements, focusing on inverse problems formulated in terms of Fredholm integral equations of the first kind.

2.2. FBG sensor model

Coupled-mode equations [12] were used in the simulation of the spectral response of the Bragg grating.

The white light is the sensor model input (the light entering the grating). The input can be expressed as $R(-L/2)$. The output of the model is the light transmitted through the grating (grating's transmission spectrum), which can be expressed as $R(+L/2)$. The model parameters are as follows: the grating length L, the "DC" self-coupling coefficient σ, and the coupling coefficient k.

There is no input signal that is incident from the right-hand side of the grating, *i.e.* $S(+L/2)=0$, but there is a known signal value that is incident from the left side of the grating, *i.e.* $R(-L/2)=1$.

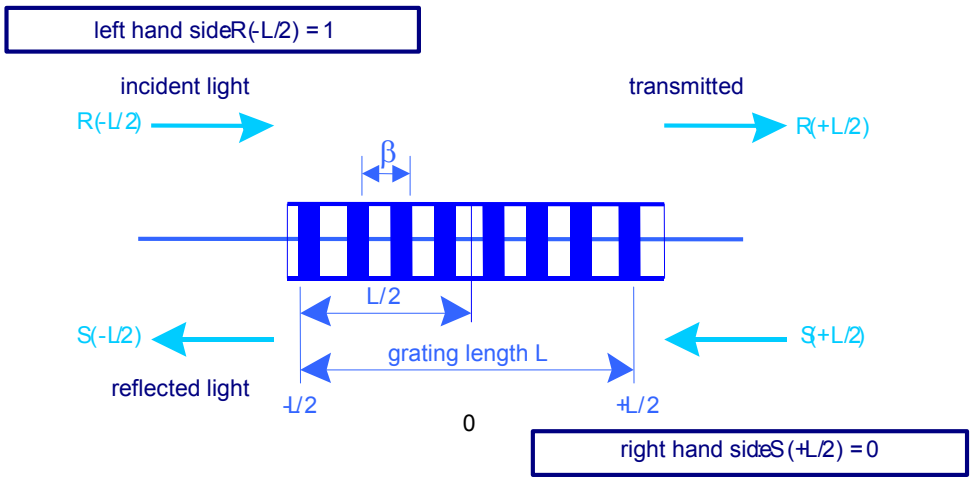

Fig. 2. The initial condition and calculation of the grating response to input field.

The grating is represented by the transfer matrix F_M. The light propagation process can be described by:

$$\begin{bmatrix} R(+L/2) \\ S(-L/2) \end{bmatrix} = F_M \cdot \begin{bmatrix} R(-L/2) \\ S(+L/2) \end{bmatrix}. \tag{2}$$

$S(-L/2)$ is the signal reflected from the grating and the F_M matrix can be expressed as follows:

$$F_M = \begin{bmatrix} \cosh(\gamma_B L) - i\frac{\sigma}{\gamma_B}\sinh(\gamma_B L) & -i\frac{k}{\gamma_B}\sinh(\gamma_B L) \\ i\frac{k}{\gamma_B}\sinh(\gamma_B L) & \cosh(\gamma_B L) + i\frac{\sigma}{\gamma_B}\sinh(\gamma_B L) \end{bmatrix}. \quad (3)$$

The individual elements of the F_M matrix can be described as follows.

The general "DC" self-coupling coefficient σ can be represented by [12]:

$$\sigma = \delta + \overline{\sigma} - \frac{1}{2}\frac{d\varphi}{dz}, \quad (4)$$

where $\frac{1}{2}\frac{d\phi}{dz}$ describes a possible chirp of the grating period, and ϕ is the grating phase. The detuning parameter δ can be represented by:

$$\delta = \beta - \frac{\pi}{\lambda} = \beta - \beta_D = 2\pi n_{eff}\left(\frac{1}{\lambda} - \frac{1}{\lambda_D}\right), \quad (5)$$

where $\lambda_D = 2n_{eff}\Lambda$ is the design wavelength for Bragg reflectance. For very weak gratings where ($\delta n_{eff} \to 0$) we obtain:

$$\overline{\sigma} = \frac{2\pi}{\lambda}\overline{\delta n_{eff}}, \quad (6)$$

where $\overline{\delta n_{eff}}$ is the background refractive index change.

The coupling coefficient $k(z)$ can be represented by:

$$k(z) = \frac{\pi}{\lambda}\delta n(z)\, g(z)\, v, \quad (7)$$

where $g(z)$ is the function of apodization, and v is the fringe visibility. The coupling coefficient $k(z)$ is proportional to the modulation depth of the refractive index:

$$\Delta n(z) = \delta n(z) g(z).$$

In our case the grating was apodized and the apodization profile was given by the grating producer (Welltech Instrument). The simulated grating apodization function was as follows:

$$g(z) = \exp\left[-a\left(\frac{z - \frac{L}{2}}{L}\right)^2\right];\ z \in [0, L], \quad (8)$$

where a is the Gauss function width parameter and in our case $a = 80$.

γ_B can be expressed by the following equations:

$$\gamma_B = \sqrt{k^2 - \sigma^2} \quad k^2 > \sigma^2 \quad (9)$$

$$\gamma_B = i\sqrt{\sigma^2 - k^2} \quad k^2 < \sigma^2 \quad (10)$$

2.3. Selection and description of the algorithm applied

In the first part of the study we generated a hypothetical strain distribution curve and then we checked how individual algorithms were recovering this specific curve. We used the following algorithms for the objective function minimization: the Newton algorithm, the Gauss-Newton algorithm, the conjugate gradient algorithm, the Levenberg-Marquardt algorithm, the genetic and simulated annealing algorithm. We found that for the Bragg grating definitely the best results were obtained when the simulated annealing algorithm was applied. Our criterion for the algorithm choice was the relative root mean squared error value of the strain distribution. Because of the lowest value of this error, the simulated annealing algorithm was chosen and other algorithms were rejected.

Due to the concise nature of this article we concentrate specifically on the cooling scheme of the simulated annealing algorithm. In our case the Otten cooling scheme gave the best results.

The decrement rule obtained by Otten *et al*. was proposed as follows [13]:

$$T_{k+1} = T_k - \frac{1}{M_k} \cdot \frac{T_k^3}{\sigma^2 T_k} \tag{11}$$

where: T_{k+1} is the temperature in the next iteration (next step), and M_k is given by:

$$M_k = \frac{C_{max} + T_k \cdot ln(1+\delta)}{\delta^2(T_k) \cdot ln(1+\delta)} \cdot T_k \tag{12}$$

where δ is a small real number, and C_{max} is an estimation of the maximum value of the objective function.

2.4. Experiments

Strain distribution of a specimen can be recovered on the basis of the distribution of the linear relative size change in the measured area. The research already carried out led to the use of information from the measured and modelled spectrum which was processed onto the real strain – the so-called inverse problem. The instrument which enables steel specimens stretching was designed and constructed for laboratory measurements. Fibre Bragg gratings were glued on specimens. Specimen elongations moving to the grating cause its period changes which changes the grating spectrum that could be recovered with the use of a photo spectrometer. The grating spectra carry information about the strain distribution even when it is repeatedly diverse on the measured length.

In order to obtain supposed strain distributions in the measured area different specimen shapes were used. Since we knew the specimen's cross-section and load, we calculated the strain in many points along the specimen and the Bragg grating. We used the finite element method – FEM [14] for our calculations. Fig. 3 shows specimens with the FEM mesh (real dimensions). As can be seen the mesh is condensed in the narrowing places.

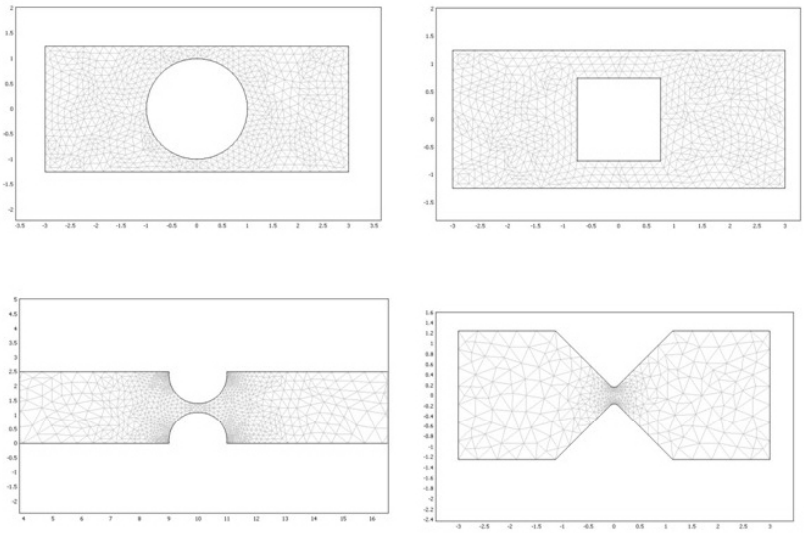

Fig. 3. The mesh of finite physical elements averaging the specimens' physical state.

The 3-D analysis provided complete information about the strain values of a specimen, glue and the grating. Calculation results for the three dimensions are shown in the following figures. The FEM mesh is three-dimensional (Fig. 4). As can be seen, the whole specimen-glue-FBG system is covered by the finite element method. The size of the FEM mesh in the glue and the Bragg grating in the fibre is smaller than the FEM mesh size in the specimen.

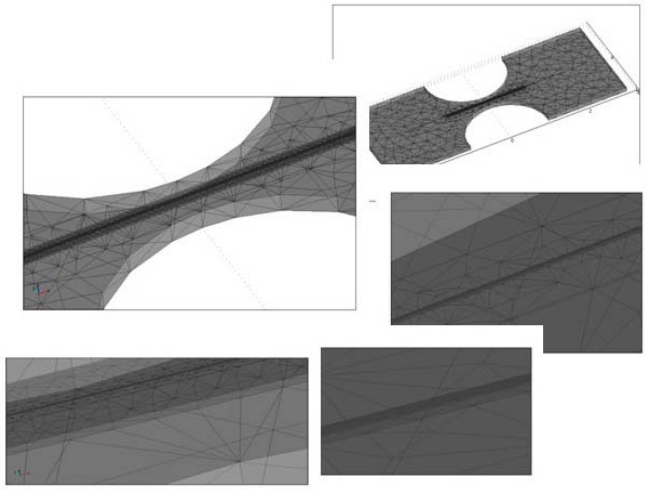

Fig. 4. 3D FEM mesh.

The FEM analysis allowed a theoretical calculation of the Bragg grating strain values [15] for every shape of the measured specimens. The theoretical strain distribution (which was calculated with the use of the FEM) was depicted in shared characteristics in a further part of this article. This strain distribution was presented together with the distribution determined by the solution of the inverse problem.

The research was conducted on a constructed laboratory system, which is shown in Fig. 5.

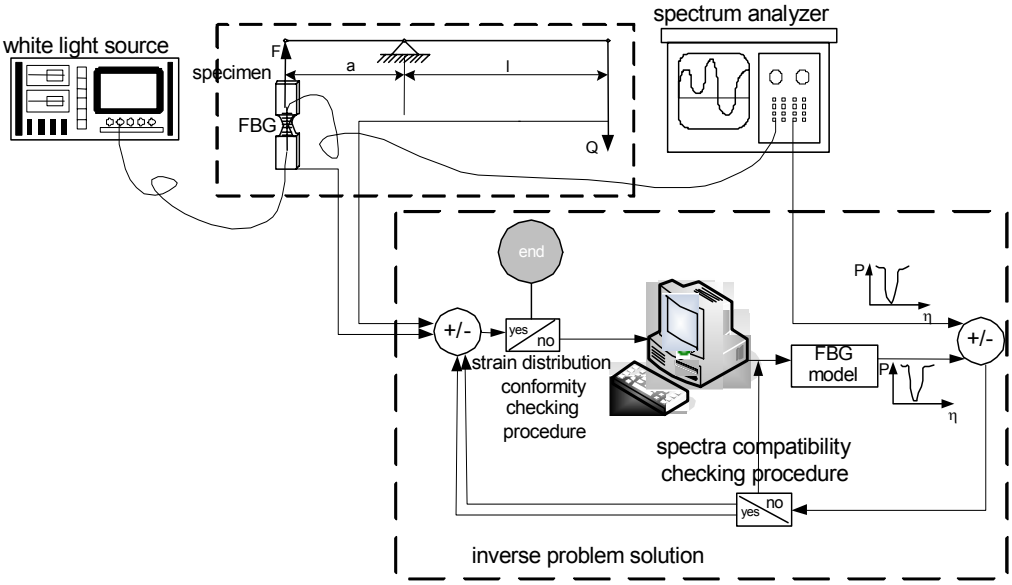

Fig. 5. The diagram of a laboratory system for the strain distribution recovery with the use of the Bragg gratings.

The light of the wavelength in the range of 400-1700 nm (the white light source YOKOGAWA AQ-4305) was directed to an optical fibre with the FBG. The grating was glued to the specimen and the specimen was stretched by the force F using the laboratory system for strain generation. The light (its modified spectrum) passed through the lengthened grating and was then directed to an optical spectrum analyzer (ANDO AQ-6315B). At the same time, strain distribution was generated at random with the use of the simulated annealing algorithm. This accidental distribution was then introduced to the model of the Bragg grating. On the basis of the model and the accidental strain distribution, the transmission spectrum of the grating was calculated. The real (from the spectrum analyzer) and model spectra were then compared and the objective function value was calculated. If the spectral characteristics were not compatible, new values of the strain distribution were selected (according to the simulated annealing algorithm). The whole process was repeated until we obtained the predetermined accuracy and a specific (suitably small) value of the objective function. The distribution leading to the objective function minimization was the correct distribution and it was the best match to the real one. The next step was the distribution compatibility checking process. The distribution recovered (with the use of the algorithm) was compared with the theoretical distribution resulting from the force F and the known shape of the specimen.

The measure of the theoretical and recovered characteristic conformity is the relative root mean squared error value δ:

$$\delta = \sqrt{\frac{1}{N}\sum_{i=1}^{N}\left(\frac{\varepsilon_i^{a\lg} - \varepsilon_i^{MES}}{\varepsilon_i^{MES}}\right)^2}, \tag{13}$$

where: ε_i^{MES} is the theoretical strain value and $\varepsilon_i^{a\lg}$ is the recovered strain value which is calculated with the use of the simulated annealing algorithm, N is the number of points in which the strain values are calculated. In this case N=10.

3. Direct measurements and calculation results

Figs 6-9 show shapes of specimens used and Figs 10-13 present strain distributions of these specimens for the theoretical case (calculated on the basis of the load, specimens' geometry and specimen material) and the simulated case (recovered from indirect measurements in the laboratory system).

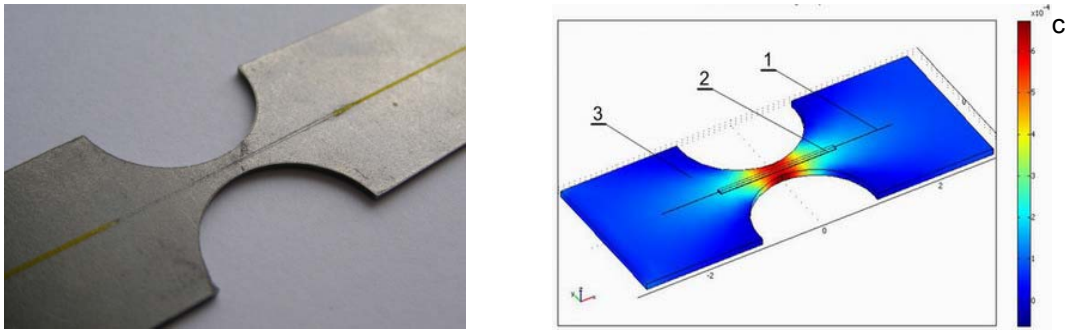

Fig. 6. The system measured: 1 – optical fibre with the FBG, 2 – glue, 3 – specimen number 1.

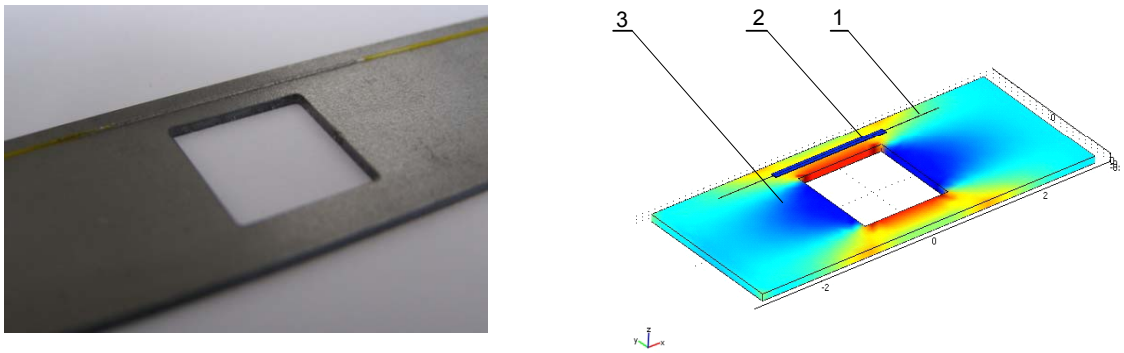

Fig. 7. The system measured: 1 – optical fibre with the FBG, 2 – glue, 3 – specimen number 2.

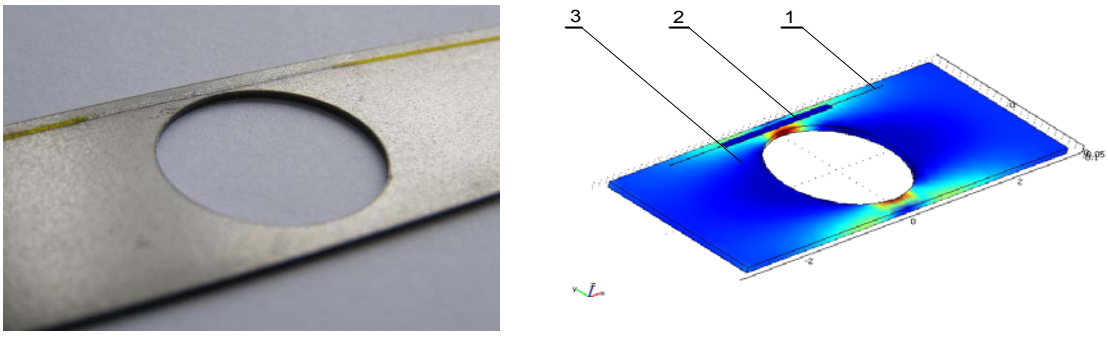

Fig. 8. The system measured: 1 – optical fibre with the FBG, 2 – glue, 3 – specimen number 3.

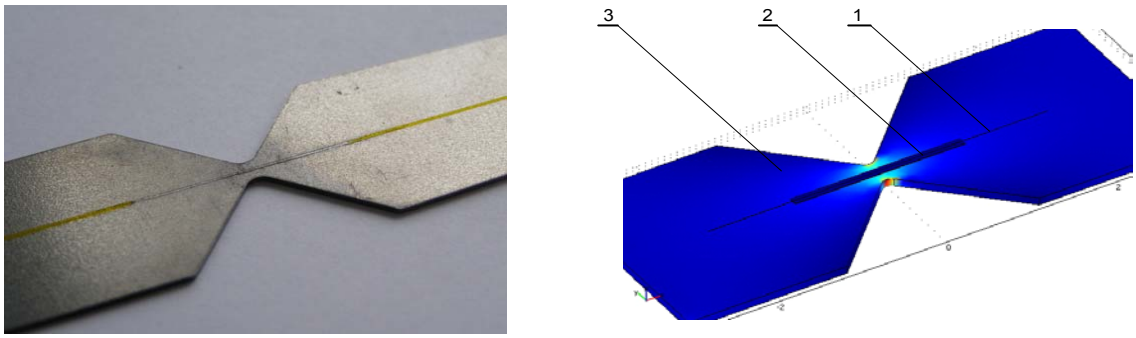

Fig. 9. The system measured: 1 – optical fibre with the FBG, 2 – glue, 3 – specimen number 4.

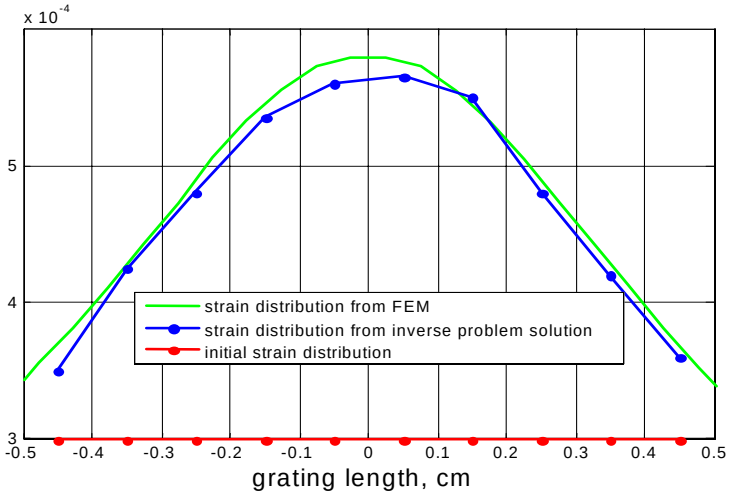

Fig. 10. Strain distributions in the grating: from FEM (green line), initial (red line) and recovered with the use of the simulated annealing algorithm (blue line) for the specimen number 1.

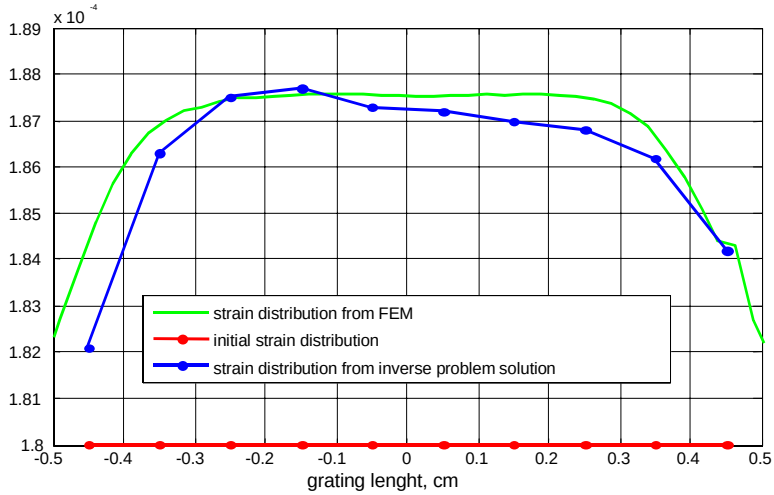

Fig. 11. Strain distributions in the grating: from FEM (green line), initial (red line) and recovered with the use of the simulated annealing algorithm (blue line) for the specimen number 2.

Results presented in Fig. 10 indicate that the proposed method using the simulated annealing algorithm showed convergence of the resolution, regardless of established initial

values. In the case of the specimen shape presented in Fig. 6 (specimen number 1) the relative root mean squared error calculated according to equation (13) was δ=0,094. The δ error value for specimen number 2 was 10 times smaller than the error value for the specimen number 1. The error value depends also on strain values. The next step was measurements of the specimen number 3, the shape of which was shown in Fig. 8. As in previous specimens the grating was glued onto the specimen in the narrowing place. Fig 8 shows the method of location of the Bragg grating on the specimen.

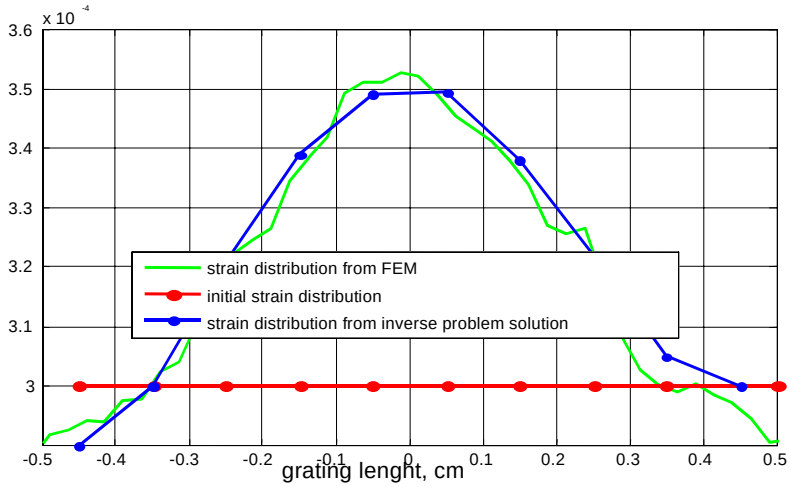

Fig. 12. Strain distributions in the grating: from FEM (green line), initial (red line) and recovered with the use of the simulated annealing algorithm (blue line) for the specimen number 3.

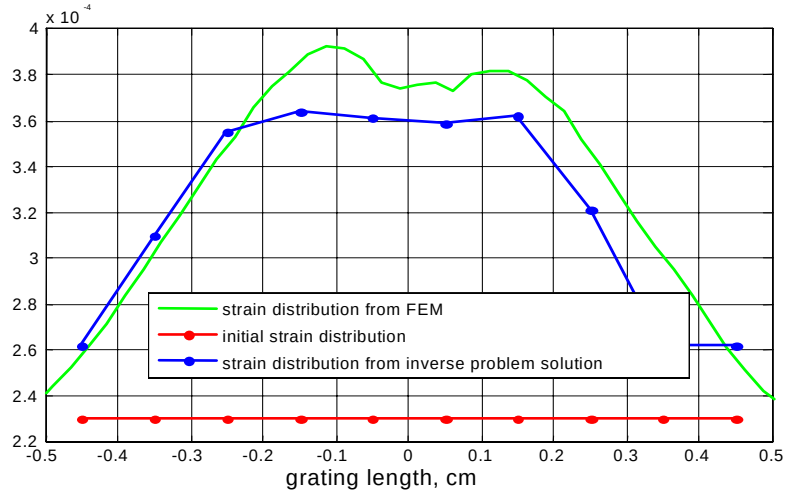

Fig. 13. Strain distributions in the grating: from FEM (green line), initial (red line) recovered with the use of the simulated annealing algorithm (blue line) for the specimen number 4.

Results of the adaptation of the model presented in this article to experimental data for a concrete strain profile were outlined in an article [16]. In that study the grating spectra from the measurements and from the grating model were shown in one graph.

Measurements and calculations results are presented in Fig. 12. As in previous measurements – also in the case of specimen number 3 – the strain distribution was determined according to the proposed method. In this case error δ was 0.046.

Specimen number 4 was the last we measured. The shape of this specimen was shown in Fig. 9. Also in this case the Bragg grating was glued in the narrowing place on the specimen. Measurements and calculations results for specimen number 4 are put together in Fig. 13. For specimen number 4 the distinct convergence between the recovered and real strain distribution could be seen – as in specimens 1, 2 and 3. The error of the strain distribution determination which was calculated according to equation (13) was δ=0.191. As can be seen (on the basis of characteristics in Figs 10-13) there is a relationship between the error δ and the shape and character of the strain distribution. The error value for specimens 1 to 3 did not exceed 0.05. The error achieved the value of 0.191 only for specimen number 4 which was caused by the shape of the real strain distribution. The strain distribution shape for specimen number 4 is the most diverse and this results in the highest δ error.

Table 1 shows the calculated relative accuracies of the strain distribution.

Table 1. Relative root mean squared error values for individual specimens.

specimen number	1	2	3	4
relative root mean squared error δ	0,094	0,009	0,046	0,191

The differences in strain distributions from FEM and SA also depend on the FEM because in this method the continuous space is divided into finite elements.

4. Summary

The results of laboratory measurements and numerical simulations presented here indicate that it is possible to apply the inverse analysis to determine the strain distribution with the use of fibre Bragg grating sensors.

The forward problem could be realized by the development and validation of the mathematical model of the Bragg grating sensor.

It is possible to conduct computer simulations with the use of numerical algorithms which realize calculations according to the mathematical structure of the Bragg grating model and which respect values of all model parameters.

The simulated annealing algorithm we used shows very small result sensitivity to the established initial point.

The application of regularization seems to be a desired next step in parameter estimations of the Bragg grating model.

References

[1] A. Othonos, K. Kalli: *Fibre Bragg gratings: fundamentals and applications in telecommunications and sensing.* Artech House, 1999, pp. 21-45.

[2] G. Hongwei, L. Hongmin, L. Bo, Z. Hao, L. Jianhua, C. Ye, Y. Shuzhong, Z. Weigang, K. Guiyun, D. Xiaoyi: "A novel fibre Bragg grating sensors multiplexing technique". *Optics Communications,* no. 251, 2005, pp. 361-366.

[3] M. Mulle, R. Zitoune, F. Collombet, L. Robert, Y.-H. Grunevald: "Embedded FBGs and 3-D DIC for the stress analysis of a structural specimen subjected to bending". *Composite Structures,* no. 91, 2009, pp. 48-55.

[4] C. Frias, O. Frazão, S. Tavares, A. Vieira, A.T. Marques, J. Simões: "Mechanical characterization of bone cement using fibre Bragg grating sensors". *Materials and Design*, no. 30, 2009, pp. 1841-1844.

[5] M Majumder, T. K. Gangopadhyay, A. K. Chakraborty, K. Dasgupta, D.K. Bhattacharya: "Fibre Bragg gratings in structural health monitoring – Present status and applications". *Sensors and Actuators A,* no. 147, 2008, pp. 150-164.

[6] C.A. Ramos, R. de Oliveira, A.T. Marques: "Design of an optical fibre sensor patch for longitudinal strain measurement in structures". *Materials and Design*, no. 30, 2009, pp. 2323-2331.

[7] J. Botsis, L. Humbert, F. Colpo, P. Giaccari: "Embedded fibre Bragg grating sensor for internal strain measurements in polymeric materials". *Optics and Lasers in Engineering*, no. 43, 2005, pp. 491-510.

[8] K.S.C. Kuang, R. Kenny, M.P. Whelan, W.J. Cantwell, P.R. Chalker: "Embedded fibre Bragg grating sensors in advanced composite materials". *Composites Science and Technology,* no. 61, 2001, pp. 1379-1387.

[9] W.Y. Li, C.C. Chenga, Y.L. Lo: "Investigation of strain transmission of surface-bonded FBGs used as strain sensors". *Sensors and Actuators A*, no. 149, 2009, pp. 201-207.

[10] A.G. Polak, J. Mroczka: "Indirect measurements of the complex objects characteristics". *Problems of the electronic and photonic metrology*, Oficyna Wydawnicza Politechniki Wrocławskiej, Wrocław 2008, pp. 16-41. (in Polish).

[11] J. Mroczka, D. Szczuczyński: "Inverse problems formulated in terms of first-kind Fredholm integral equations in indirect measurements". *Metrol. Meas. Syst*., vol. XVI, no. 3, 2009, pp. 333-357.

[12] R. Kashyap: "Fibre Bragg gratings". *Optics and photonics*, Academic Press, 1999.

[13] E. Triki, Y. Collette, P. Siarry: "A theoretical study on the behavior of simulated annealing leading to a new cooling schedule". *European Journal of Operational Research*, no. 166, 2005, pp. 77-92.

[14] O.C. Zienkiewicz, R.L. Taylor: *The Finite Element Method. The Basis*, vol. 1, Oxford, Butterworth-Heinemann, 2000.

[15] R.A. Oliveira, P.T. Neves Jr., J.T. Pereira, A.A.P. Pohl: "Numerical approach for designing a Bragg grating acousto-optic modulator using the finite element and the transfer matrix methods". *Optics Communications,* no. 281, 2008, pp. 4899-4905.

[16] W. Wójcik, P. Kisała, S. Cięszczyk: "Wykorzystanie czujnika ze światłowodową siatką Bragga do analizy połączeń klejowych". *Elektronika,* vol. XLIX, no. 6, 2008, pp. 82. (in Polish)